Cold collisions of rovibrationally excited D₂ molecules

James F. E. Croft

The Dodd-Walls Centre for Photonic and Quantum Technologies, Dunedin 9016, New Zealand and Department of Physics, University of Otago, Dunedin 9016, New Zealand

Pablo G. Jambrina

Departamento de Química Física, Universidad de Salamanca, Salamanca 37008, Spain

F. Javier Aoiz

Departamento de Química Física, Universidad Complutense, Madrid 28040, Spain

Hua Guo

Department of Chemistry and Chemical Biology, University of New Mexico, Albuquerque, New Mexico 87131, USA

N. Balakrishnan

Department of Chemistry and Biochemistry, University of Nevada, Las Vegas, Nevada 89154, USA

The H_2+H_2 system has long been considered as a benchmark system for ro-vibrational energy transfer in bimolecular collisions. However, most studies thus far have focused on collisions involving H_2 molecules in the ground vibrational level or in the first excited vibrational state. While H_2+H_2/HD collisions have received wide attention due to the important role they play in astrophysics, D_2+D_2 collisions have received much less attention. Recently, Zhou et al. [Nat. Chem. 14 658 (2022)] examined stereodynamic aspects of rotational energy transfer in collisions of two aligned D_2 molecules prepared in the v=2 vibrational level and j=2 rotational level. Here, we report quantum calculations of rotational and vibrational energy transfer in collisions of two D_2 molecules prepared in vibrational levels up to v=2 and identify key resonance features that contribute to the angular distribution in the experimental results of Zhou et al. The quantum scattering calculations were performed in full dimensionality and using the rigid-rotor approximation using a recently-developed highly-accurate six-dimensional potential energy surface for the H_4 system that allows descriptions of collisions involving highly vibrationally excited H_2 and its isotopologues.

I. INTRODUCTION

Bimolecular collisions involving diatomic molecules are topics of active investigation due to the continuing interest in cooling and trapping of molecules and their applications in sensing, precision spectroscopy, quantum information processing, and ultracold chemistry [1–12]. Heteronuclear alkali-metal dimers due to their easily accessible optical transitions and open-shell molecules with their nearlydiagonal Franck-Condon factors permitting laser cooling and trapping are the molecules of choice in these experiments [13–17]. These systems are largely not amenable to full-quantum scattering calculations due to their high density of states, chemically reactive nature, and possible non-adiabatic effects. Thus, most theoretical studies of cold and ultracold diatom-diatom collisions involving these systems have resorted to approximate models or not explicitly considered geometries in which all four atoms are in close proximity [18, 19]. From a computational perspective, lighter molecular systems are preferable for explicit comparisons and benchmarking between theory and experiment. However, molecules such as H₂ and D₂ that serve as benchmark systems for bimolecular collisions are not amenable to laser cooling or other molecule cooling methods that rely on properties such as a permanent dipole moment or magnetic moment.

In the last several years, Mukherjee, Zare, and coworkers have reported a series of experiments on rotational quenching of optically state prepared (and aligned) HD in collisions with unpolarized H_2 , D_2 and He [20–26]. More recently, they have extended this approach to D_2 +He [23, 24] and D_2 + D_2 collisions [26] in which the D_2 molecule is prepared in the v=2 vibrational level and j=2 rotational level. A scheme to optically prepare D_2 molecules in the v=4 vibrational level has also been proposed [25]. For the first time, rotational transfer in $D_2(v = 2, j = 2) + D_2(v = 2, j = 2)$ collisions was reported in which state-preparation and the alignment of both D₂ molecules were controlled using the Starkinduced adiabatic Raman passage (SARP) technique [26]. Additionally, co-expansion of the molecules (or the two colliding species) in the same molecular beam allows relative collision energies to be reduced to the vicinity of 1 K. This permits studies of cold molecular collisions involving H₂, HD and D₂ in the 1 K range where collisions are dominated by a few low-lying partial waves in the incident channel. Further, the SARP method can align the molecular bond axis relative to the initial relative velocity vector allowing stereodynamic studies of molecular collisions in a regime where collision dynamics is dominated by isolated partial wave resonances. For rotational transfer in $D_2(v=2, j=2) + D_2(v=2, j=2)$ collisions

Zhou et al. concluded that the angular distribution is primarily governed by a l=2 partial wave resonance in the incident channel at around 1 K. However such conclusions, obtained by fitting outgoing partial wave scattering amplitudes to experimental angular distributions, may not tell the full story especially due to the relatively broad collision energy distribution of the molecules in the beam. In fact, as discussed in this manuscript and elsewhere, our results show that several resonances contribute in this regime, with dominant contributions from an l=4 partial wave resonance [27].

While H_2+H_2 and H_2+HD collisions have been the topics of numerous prior investigations, D₂+D₂ collisions have received much less attention. A survey of previous studies of H₂+H₂ and H₂+HD collisions was provided in our recent work that reported a new full-dimensional potential energy surface (PES) for the H₄ system [28]. Early studies of H₂+H₂ collisions have used the rigid rotor (RR) approximation. This includes the seminal work of Green [29] that reported one of the earliest calculations of rotational transitions in H₂+H₂ collisions using the analytic interaction potential developed by Zarur and Rabitz [30]. This is followed by theoretical studies of Flower [31] and Flower and Roueff [32, 33] using the interaction potential of Schwenke [34]. Lee et al. [35] reported rotational transitions using a more accurate four-dimensional (4D) PES of Diep and Johnson [36, 37], referred to as the DJ PES.

The first full-dimensional quantum calculations of rovibrational transitions in H₂+H₂ collisions were reported by Pogrebnya and Clary [38] within the coupled-states (CS) approximation using the six-dimensional (6D) potential energy surface of Bothroyd et al. [39], referred to as the BMKP PES. However, the BMKP PES yielded rate coefficients that are too large compared to experimental results owing to the presence of high-order anisotropic terms in the interaction potential and its less accurate description of the long-range interaction. A restricted version of this PES, referred to as BMKPE PES [38], that excluded high-order anisotropic terms, yielded results in better agreement with experiments. Quantum wave packet calculations of ro-vibrational transitions within the CS approximation were also reported by Lin and Guo [40–42] on the BMKP PES. Gatti et al. [43] and Panda et al. [44] reported cross sections for rotational transitions in $para-H_2+para-H_2$ and $ortho-H_2+para-H_2$ collisions using the multiconfiguration time-dependent Hartree (MCTDH) algorithm and the BMKP PES. The BMKP PES was also used in full-dimensional coupledchannel (CC) calculations of ro-vibrational transitions in H₂+H₂ collisions [45, 46]. An interaction potential developed by Hinde [47] has been used in a number of recent CC studies of rovibrational transfer in H₂+H₂ collisions by Quéméner et. al [48–50] that yielded good agreement with experiments for both pure rotational and ro-vibrational transitions. A 4D interaction potential developed by Patkowski et al. [51] that employed a larger basis set than the Hinde PES also yielded results in good agreement with

experiments for pure rotational transitions. Extensive calculations of rotational transitions involving collisions of highly rotationally excited H₂ molecules were reported by Wan et al. [52] employing the 4D PES of Patkowski et al. This potential was also used in recent studies of H₂+H₂ collisions by Hernández et al. [53]. None of the H₂-H₂ PESs discussed above are constructed to study collisions of H₂ and its isotopologues with vibrational excitation beyond the v=1 vibrational level. Here, we report rotational and vibrational transitions in collisions involving D_2 molecules for vibrational levels v = 0-2 using a recently reported full-dimensional H₄ PES [28]. This potential was chosen in this work because it covers a large configuration space and is constructed specifically for collisions between molecules in excited vibrational levels up to v = 10.

Cross section measurements for elastic scattering in n- D_2+n - D_2 and o- D_2+o - D_2 collisions were first reported by Johnson, Grace, and Skofronick [54] for relative velocities in the range of 190-1000 m/s (~ 4 -121 K). Accompanying theoretical calculations by the same authors using a model potential developed by Schaefer and Meyer [55] revealed a three peak structure arising from orbital resonances l=4 near 170 m/s, l=5 near 280 m/s, and l=6 near 400 m/s. While these resonance peaks were not resolved in the experiments the minimum between the l=4 and l=5 resonances was reproduced by the experimental data. We are not aware of any subsequent theoretical studies that reproduced these resonance features or provided more rigorous comparisons with experiments. To the best of our knowledge the only theoretical work on D₂+D₂ inelastic collisions corresponds to recent work of Montero and Péréz-Ríos [56] within a rigid rotor formalism using the PES of Diep and Johnson [36, 37] to evaluate bulk viscosity and rotational relaxation rates.

The paper is organized as follows. In Sec. II, we provide a brief description of the scattering calculations. In Sec. III A we present results for elastic collisions between D_2 molecules in their ground vibrational state, and compare with the experimental results of Johnson *et al.* [54]. In Sec. III B we present rotational quenching cross sections for collisions between D_2 molecules in excited vibrational states, focusing on D_2 in v=2 to compare with the experimental results of Zhou *et al.* [26]. Finally we conclude with a summary of our findings in Sec. IV.

II. METHODS

A. Potential Energy Surface

Computations were performed using the full-dimensional H_4 PES of Zuo *et al.* [28]. Fig. 1 shows the dominant terms in the potential expansion with the D_2 distances fixed at their vibrational averaged values of $r = 1.435 \, a_0$ for the ground ro-vibrational state. The angular dependence of the potential was expanded as

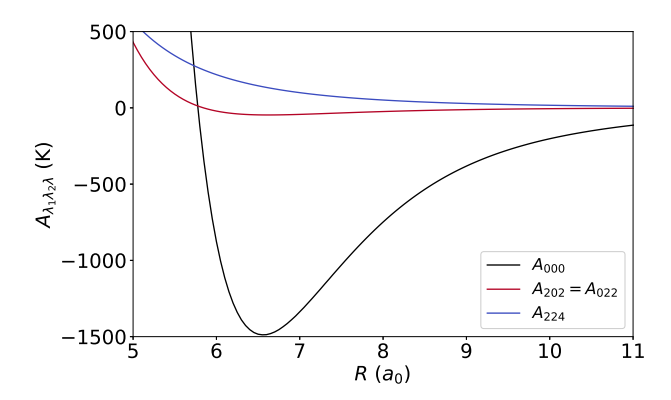


FIG. 1. Dominant terms in the spherical harmonic expansion of the angular dependence of the interaction potential as a function of the distance between the two diatoms.

$$U(\vec{r_1}, \vec{r_2}, \vec{R}) = \sum_{\lambda} A_{\lambda}(r_1, r_2, R) Y_{\lambda}(\hat{r}_1, \hat{r}_2, \hat{R}), \quad (1)$$

with

$$Y_{\lambda}(\hat{r}_{1}, \hat{r}_{2}, \hat{R}) = \sum_{m} \langle \lambda_{1} m_{1} \lambda_{2} m_{2} | \lambda_{12} m_{12} \rangle Y_{\lambda_{1} m_{1}}(\hat{r}_{1})$$

$$\times Y_{\lambda_{2} m_{2}}(\hat{r}_{2}) Y_{\lambda_{12} m_{12}}^{*}(\hat{R}), \tag{2}$$

where $\lambda \equiv \lambda_1 \lambda_2 \lambda_{12}$, $m \equiv m_1 m_2 m_{12}$, $\vec{r_1}(r_1, \hat{r}_1)$ and $\vec{r_2}(r_2, \hat{r}_2)$ denote the vector connecting the two Ds in each diatom while $\vec{R}(R, \hat{R})$ denotes the vector joining the centers of mass of the two molecules. For the scattering calculations it was found that λ up to six was sufficient to converge the cross sections for all transitions considered here.

B. Scattering calculations

Scattering calculations were performed in fulldimensionality using a modified version of the TwoBC code [57]. The methodology for the collision between two indistinguishable molecules is well established and has been outlined in detail elsewhere [45, 46, 49, 58–61], and been applied to other similar systems involving various isotopologues of hydrogen [28, 46, 50, 62–65]. Here we briefly review the methodology in order to define notation. The scattering calculations are performed within the time-independent close-coupling formalism yielding the usual asymptotic S matrix [58]. For convenience, we label each asymptotic channel by the combined molecular state (CMS) $\alpha \equiv v_1 j_1 v_2 j_2$, where v and j are the vibrational and rotational quantum numbers respectively and the subscript refers to each molecule. Since the molecules are indistinguishable we follow the "well ordered" states classification, and include states where $v_1 > v_2$ or when $v_1 = v_2, j_1 \ge j_2$ [59–61].

The integral cross section for state-to-state rovibrationally inelastic scattering for a given exchange permutation, ϵ_P , and collision energy E, is given by,

$$\sigma_{\alpha \to \alpha'}^{\epsilon_P} = \frac{\pi (1 + \delta_{v_1 v_2} \delta_{j_1 j_2}) (1 + \delta_{v_1' v_2'} \delta_{j_1' j_2'})}{(2j_1 + 1) (2j_2 + 1) k_{\alpha}^2}$$

$$\times \sum_{J, j_{12}, j_{12}', l, l'} (2J + 1) |T_{\alpha l j_{12}, \alpha' l' j_{12}'}^{J \epsilon_P}|^2,$$
(3)

where $k^2 = 2\mu E/\hbar^2$, μ is the reduced mass of the molecule-molecule system, $T^J = 1 - S^J$, l is the orbital angular momentum, J the total angular momentum ($\mathbf{J} = \mathbf{l} + \mathbf{j}_{12}$), and $\mathbf{j}_{12} = \mathbf{j}_1 + \mathbf{j}_2$. There are a number of conventions for the cross sections for collisions between indistinguishable molecules that differ by factors of 2 [60, 66–68]. The difference has been discussed by a number of authors [35, 59, 69–72], and all conventions yield the same physically observable rate. We adopt here the convention of Green [46]. The corresponding energy dependent rate coefficient is

$$k_{\alpha \to \alpha'}^{\epsilon_P} = \frac{\pi \hbar}{\mu k_{\alpha} (2j_1 + 1)(2j_2 + 1)} \times \sum_{J, j_{12}, j'_{12}, l, l'} (2J + 1) |T_{\alpha l j_{12}, \alpha' l' j'_{12}}^{\epsilon_P}|^2.$$
(4)

In general, experiments cannot select the nuclear spin state for the colliding molecules and in which case the state-to-state cross section (rate) is given by a statistically weighted sum of the exchange-permutation symmetrized cross sections (rates):

$$\sigma_{\alpha \to \alpha'} = W^+ \sigma_{\alpha \to \alpha'}^+ + W^- \sigma_{\alpha \to \alpha'}^-, \tag{5}$$

$$k_{\alpha \to \alpha'} = W^+ k_{\alpha \to \alpha'}^+ + W^- k_{\alpha \to \alpha'}^-. \tag{6}$$

The D₂ molecule consists of two spin 1 D atoms, as such for collisions between molecules in even rotational levels $W^+ = 21/36$ and $W^- = 15/36$, while for collisions between molecules in odd rotational levels $W^+ = 6/9$ and $W^- = 3/9$ [54].

Finally the experimental observable rate of molecules produced in $v'_1j'_1$ from v_1j_1 per unit time is

$$\frac{dn_{v_1j_1 \to v_1'j_1'}}{dt} = \sum_{v_2'j_2'} \sum_{v_2j_2} (1 + \delta_{v_1'v_2'} \delta_{j_1'j_2'}) k_{\alpha \to \alpha'} n_{v_1j_1} n_{v_2j_2},$$
(7

where the extra delta function accounts for the fact that each collision event produces two molecules and n_a refers to the density of molecules in state a [73, 74].

In the scattering calculations the CC equations were propagated from 3 to $103\,a_0$ with a radial step size of $0.05\,a_0$ using a log-derivative method [75]. The number of points in the radial coordinate for each diatom for the discrete variable representation was 24; the number of points in the angular coordinate θ between \vec{R} and \vec{r} for each diatom for the Gauss-Legendre quadrature was 14; the number of points in the dihedral angle between θ_1 and

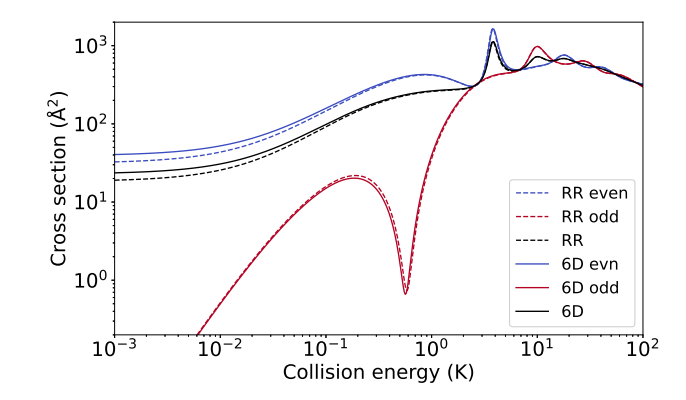


FIG. 2. Elastic cross section as a function of the collision energy for ortho-D₂ + ortho-D₂ collisions. Both the total cross section as well as the contribution from each exchange permutation symmetry are shown.

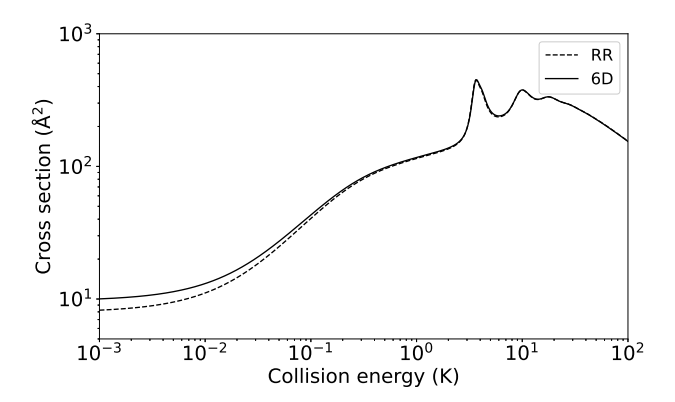


FIG. 3. Elastic cross section as a function of the collision energy for ortho-D₂ + para-D₂ collisions.

 θ_2 for the Chebyshev quadrature was 8. The rotational constant of D_2 is around 41 K, as such the $D_2(j=4)$ rotation level is around 584 K above the j=2 level while the depth of the interaction potential between two D_2 molecules is only around 30 K. The basis set contained rotational levels up to j=4 within each vibrational manifold. Scattering calculations were performed for each parity, exchange permutation symmetry and total angular momentum quantum number up to and including 16.

III. RESULTS

A. Elastic collisions between molecules in their ground vibrational state

By convention D_2 molecules in j = 0 are called *ortho*-deuterium (*ortho*- D_2) while D_2 molecules in j = 1 are called *para*-deuterium (*para*- D_2) [54]. Figs. 2, 3, and 4 show elastic scattering cross sections for *ortho-ortho* collisions (Fig. 2), *ortho-para* collisions (Fig. 3), and *para-*

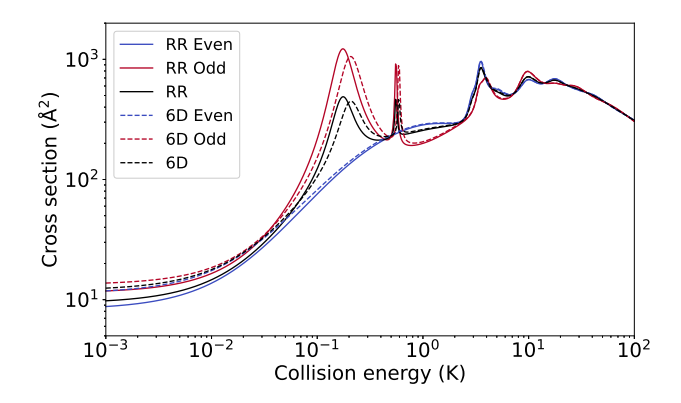


FIG. 4. Elastic cross section as a function of the collision energy for para- $D_2 + para$ - D_2 collisions. Both the total cross section as well as the contribution from each exchange permutation symmetry are shown.

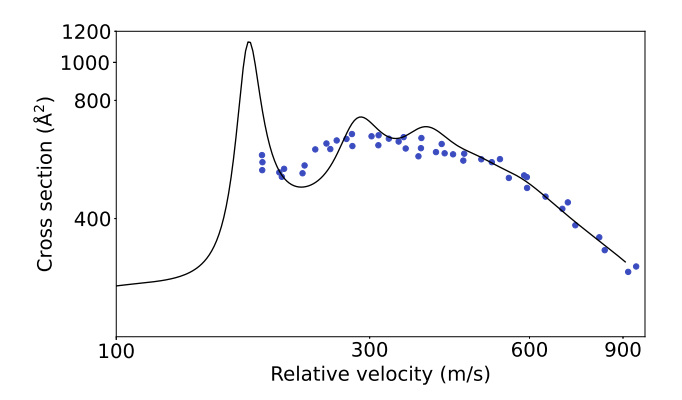


FIG. 5. Elastic cross section as a function of the relative collision velocity for ortho- $D_2 + ortho$ - D_2 collisions. The blue dots are experimental results taken from Ref. [54] which have been scaled to those from the present calculations.

para collisions (Fig. 4). Collisions between ortho-ortho and para-para correspond to indistinguishable molecules and Figs. 2 and 4 show both the statistically weighted total cross section as well as the separate even and odd exchange permutation cross sections. Collisions between ortho and para-D₂ molecules are distinguishable since they have different nuclear spins and Fig. 3 shows just the total cross section. Results are shown for the full 6D calculations as well as for rigid rotor calculations with the D₂ internuclear distance fixed at the vibrational averaged value of $r=1.435\,a_0$ for the ground ro-vibrational state. It is seen that except at low energies below $\sim 1\,\mathrm{K}$ there are no significant differences between the full 6D and the rigid rotor calculations.

Figure 5 compares the present results for *ortho-ortho* collisions with the experimental data of Johnson *et al.* [54] scaled to the present theoretical cross sections. Note that the experimental results are relative cross sections although in Ref. [54] Johnson *et al.* presented their results

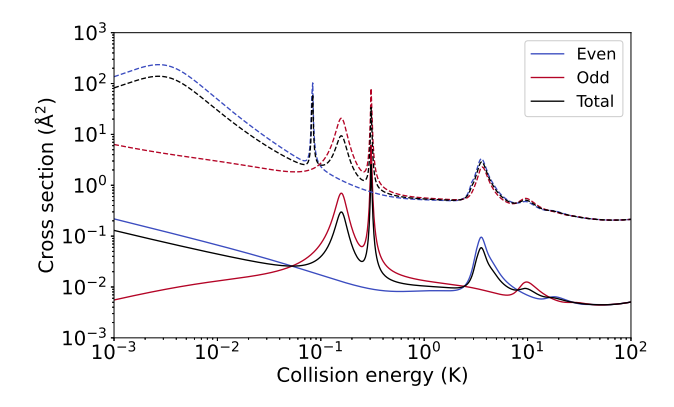


FIG. 6. Rotational quenching cross sections as a function of the collision energy for $D_2(v=0, j=2) + D_2(v=0, j=2)$ collisions. Showing both the total cross section as well as the contribution from each exchange permutation symmetry. The dashed lines are for the $0202 \rightarrow 0002$ while the solid lines are for the $0202 \rightarrow 0000$ transition.

scaled to calculations on several 1-D potentials. The present calculations are in a general good agreement with those shown in Ref. [54].

Figure 6 shows the rotational quenching cross sections for collisions between $D_2(v=0,\ j=2)$ molecules. It is seen that even at the lowest energies shown $(1\,\mathrm{mK})$, for the $0202 \to 0002$ collisions (using the CMS notation), the Wigner threshold regime ($\sigma \sim E^{-\frac{1}{2}}$ for s-wave collisions) has not been reached [76, 77]. This is generally the case when a near threshold resonance [78] is present. In this case the resonance appears as a broad peak at $3\,\mathrm{mK}$, and it is associated with l=1. This resonance is not present for the $0202 \to 0000$ transitions, for which the Wigner threshold regime is reached at $3\,\mathrm{mK}$.

B. Collisions between molecules in excited vibrational states.

It is now possible using the SARP method to achieve complete population transfer of molecules from the ground vibrational level of D_2 to excited vibrational levels [25, 26, 79]. Since SARP is a two photon process the change in vibrational level is accompanied by a $\Delta j=2$ rotational excitation. As such here we examine collisions between two D_2 molecules in the same vibrational excited state and both in j=2. Figures 7 and 8 show the rotational quenching cross sections for collisions between D_2 molecules in the first and second vibrational excited states. For collisions below 100 K our results show that it was not necessary to include basis functions corresponding to energetically closed vibrational levels.

Both Figs. 7 and 8 show the same general features, however significant differences are seen compared to the v=0 cross section shown in Fig. 6. Unlike the v=0 case, for both v=1 and v=2, the Wigner threshold

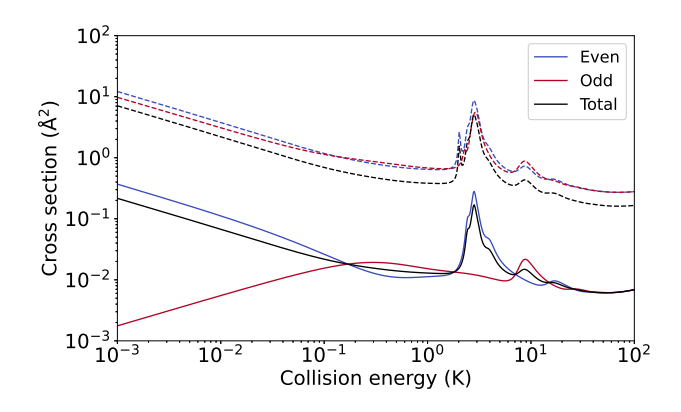
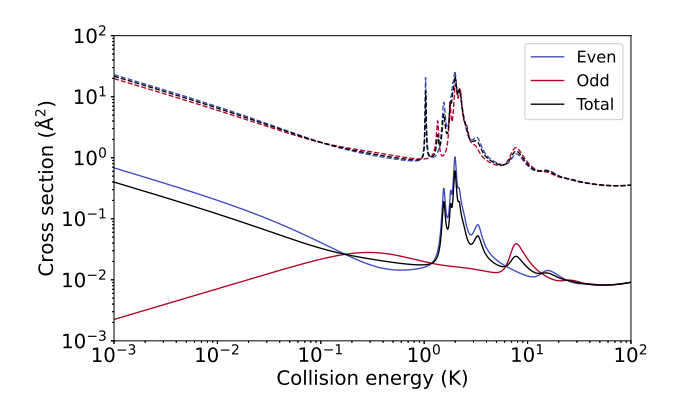


FIG. 7. Rotational quenching cross sections as a function of the collision energy for $D_2(v=1, j=2) + D_2(v=1, j=2)$ collisions. Showing both the total cross section as well as the contribution from each exchange permutation symmetry. The dashed lines are for the $1212 \rightarrow 1012$ while the solid lines are for the $1212 \rightarrow 1010$ transition.

regime is already reached by around 0.1 K. This appears to be due to the absence of a near-threshold resonance for the vibrationally excited collisions, that appear for v=0, l=1. Such resonances are very sensitive to the channel potential and off-diagonal coupling matrix elements which vary with the initial ro-vibrational level.

Figure 8 corresponds to the collisions experimentally studied by Zhou et al. [26]. They examined collisions in the $1\text{--}3\,\mathrm{K}$ range and measured the angular distribution of scattered $D_2(v'=2, j'=0)$ molecules (which are produced by both transitions shown in Fig. 8) due to collisions between aligned D₂ molecules. It can be seen that the cross sections for the double rotational quenching process are much smaller, and to a reasonable approximation can be ignored in the analysis of the experimental data. Analyzing the angular distribution they attributed the observed scattering behavior to a d-wave (l=2) shape resonance [26]. In order to gain insight into the nature of the resonances seen in Fig. 8, Fig. 9 shows the l resolved partial cross section, $\sigma^l(E)$. The dominant contribution to the total cross section over the 1–3 K is seen to be from l=4, consistent with the elastic cross sections reported by Johnson et al. [54], as well as our previous analysis [27]. The cluster of resonances at around 2 K was present also for v=0 and v=1 collisions, although in the case of v=2 it shows a dense structure which is associated with different J, for l=4. Fig. 10 shows the contribution of different total angular momentum J to the dominant two partial waves (l = 2, 4) seen in Fig. 9. It is seen that the various peaks of the broad l=4 feature are due to contributions from different total angular momentum J, while the narrow resonance at around 1 K is due to J=3alone with contributions from l=2 and 4 and is absent in the double de-excitation.

While it is possible to switch off the $1\,\mathrm{K}$ resonance by a suitable preparation of the internuclear axis of D_2 molecules, this is unlikely for the $2\,\mathrm{K}$ group of resonances,



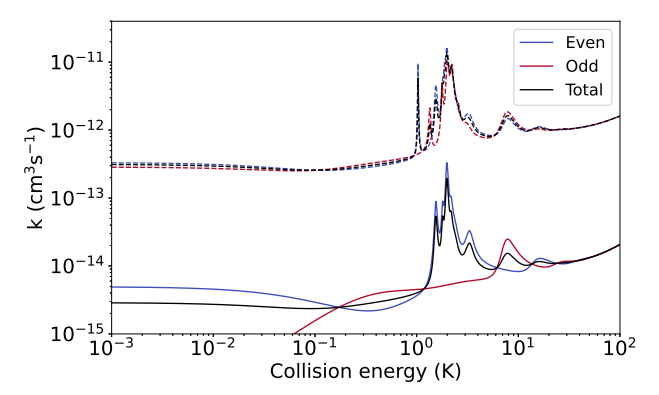


FIG. 8. Rotational quenching cross sections (upper panel) and rates (lower panel) as a function of the collision energy for $D_2(v=2,\,j=2)+D_2(v=2,\,j=2)$ collisions. Showing both the total cross section as well as the contribution from each exchange permutation symmetry. The dashed lines are for the $2222 \rightarrow 2022$ while the solid lines are for the $2222 \rightarrow 2020$ transition.

which have contributions from different values of J. However, it is still possible to modulate the strength of the resonance peaks, and it would be possible to split the overall resonance peak, as demonstrated for H+HF collisions [80].

In order to gain insight into the nature of the resonances seen in Figs. 8 and 9 we analyzed the isotropic part of the potential, evaluated with D_2 distances kept at their vibrationally averaged values of $1.575\,a_0$ (for v=2, j=2),

$$V_l(R) = V_{\rm iso} + \frac{\hbar^2}{2\mu} \frac{l(l+1)}{R^2},$$
 (8)

where $V_{\rm iso} = A_{000}/(4\pi)^{\frac{3}{2}}$. We also analyzed the effective potentials corresponding to different incoming partial waves l,

$$V^{J}(R) = \epsilon_{v_{1}j_{1}v_{2}j_{2}}$$

$$+ U^{J}_{v_{1}j_{1}v_{2}j_{2}lj_{12},v'_{1}j'_{1}v'_{2}j'_{2}l'j'_{12}}(R) + \frac{l(l+1)\hbar^{2}}{2uR^{2}}.$$

$$(9)$$

The first term is the energy of the CMS obtained by adding the asymptotic rovibrational energies of the two

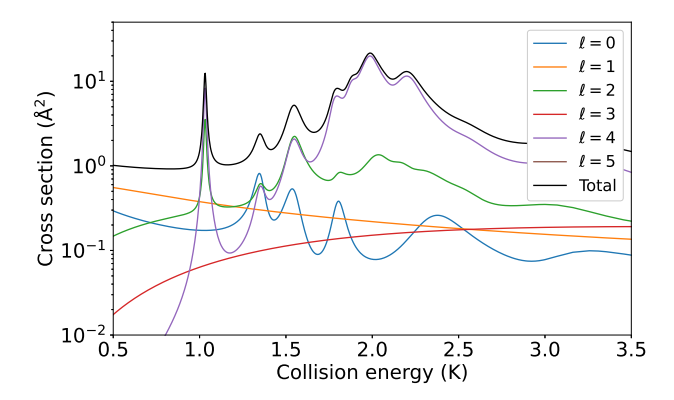


FIG. 9. l resolved partial integral cross section for the 2222 \rightarrow 2022 transition as a function of the collision energy for $D_2(v=2, j=2) + D_2(v=2, j=2)$ collisions.

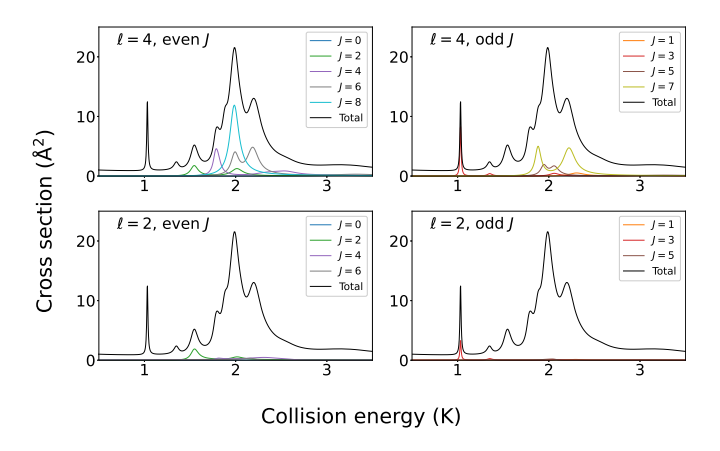


FIG. 10. l and J resolved partial integral cross sections for the 2222 \rightarrow 2022 transition as a function of the collision energy for $D_2(v=2,\,j=2)+D_2(v=2,\,j=2)$ collisions. The top two panels show the contribution from l=4 for even J (left panel) and odd J (right panel) while the bottom two panels show the contribution from l=2 for even J (left panel) and odd J (right panel).

 D_2 molecules, the second term is the potential energy matrix in the channel basis, and the third term is the centrifugal potential for the orbital angular momentum l. Fig. 11 shows both the radial potentials with the solid line showing the isotropic potential (Eq. 8) while the dashed line shows the effective potential for $v_1 = 2, j_1 =$ $2, v_2 = 2, j_2 = 2, j_{12} = 0, J = 0$ (Eq. 9). The height of the centrifugal barriers are 0.13, 0.69, 1.96, 4.21, and $7.76\,\mathrm{K}$ for l=1 to 5 for the isotropic potential (for the effective potential the barrier heights are almost identical— 0.13, 0.69, 1.96, 4.26, and 7.77 K). This suggests that in the 1–3 K region it is l=3 and 4 partial waves which will be the dominant contributions to the experimental cross section. It is clearly seen that the radial potentials differ little suggesting that using the isotropic part of the potential captures the main physics of the problem. The depth of the radial potentials increases with vibrational

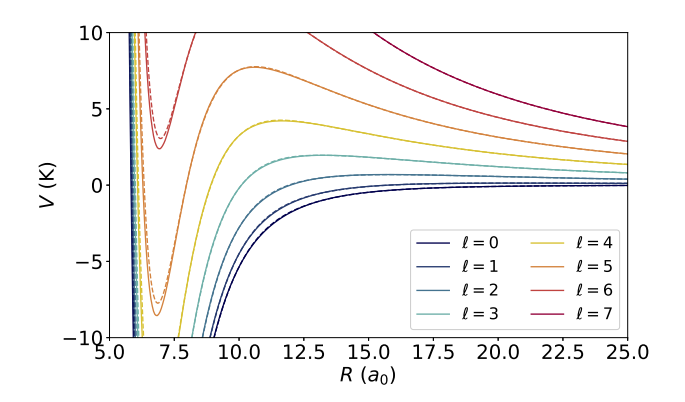


FIG. 11. Isotropic part of the $D_2 + D_2$ potential + centrifugal barriers (solid lines), effective potential for $v_1 = 2, j_1 = 2, v_2 = 2, j_2 = 2, j_{12} = 0, J = 0$ (dashed lines).

quantum number. This explains why the low energy l=1 resonance seen for the 0202 collisions (see Fig. 6) is not seen for the 1212 (see Fig. 7) or 2222 (see Fig. 8) cases since the resonance has been shifted to below threshold.

To further investigate the nature of the resonances seen in Fig 8 and 9 we performed a semiclassical WKB analysis to find the approximate locations of bound states for the system. The WKB phase was evaluated from the integral

$$\theta_{\text{WKB}} = \int dR \sqrt{2\mu (V(R) - E)/\hbar^2}, \qquad (10)$$

where the integration is carried out between the classical turning points at the energy E for the radial potentials shown in Fig. 11. The corresponding quantization condition is $\theta_{\text{WKB}} = \pi(n+\frac{1}{2})$, for the n^{th} bound state of the potential. Figure 12 shows the WKB phase as a function of the energy for each of the radial potentials shown in Fig. 11, along with a vertical line identifying the quantization condition. It can be seen that WKB predicts at most a single bound state in each channel with a bound state for l=0,1,2,3 while an above threshold quasi-bound state at around 2 K for l=4, which manifests itself as a shape resonance in the scattering experiments, in excellent agreement with the full 6D scattering results shown in Figs. 8 and 9. For l=5 there is no quasi-bound state with the WKB phase not reaching $\pi/2$ below the height of the centrifugal barrier.

This analysis shows that for these types of systems it is possible to predict the relevant partial waves that will contribute to the cross section in the 1 K range using simply the isotropic part of the potential combined with a WKB analysis. This suggests that using such an

approach to identify the relevant partial waves to inform an experimental analysis would be fruitful.

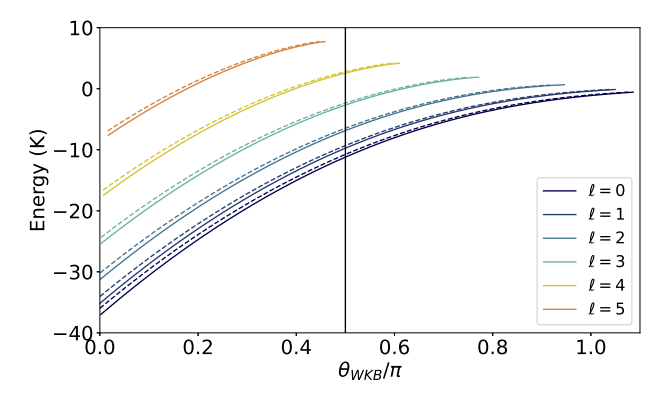


FIG. 12. The WKB phase for the radial potentials shown in Fig. 11. The vertical line shows the quantization condition for the lowest energy state.

IV. CONCLUSION

We have presented full-dimensional scattering calculations of rotational and vibrational transitions in collisions between two D_2 molecules prepared in vibrational levels v = 0–2 and rotational levels j = 0–2. Computations are performed using a recently reported full-dimensional ab initio potential energy surface for the H₄ system designed to treat collisions of highly vibrationally excited H₂ and its isotopologues. Our calculations show that resonance features in low energy collisions of two D₂ molecules below 5 K arise primarily from a l = 4 partial wave resonance, consistent with the prediction of Johnson et al. [54] for elastic collisions using an isotropic potential. For collisions between two D_2 molecules in the v=2 vibrational state and j=2 rotational state, cross sections for double rotational relaxation is found to be about two orders of magnitude smaller than that of relaxation of only one molecule.

ACKNOWLEDGMENTS

This work was supported in part by NSF grant No. PHY-2110227 (N.B.) and ARO MURI grant No. W911NF-19-1-0283 (N.B., H.G.). P.G.J. gratefully acknowledges grant PID2020-113147GA-I00 funded by MCIN/AEI/10.13039/, and F.J.A. acknowledges funding by the Spanish Ministry of Science and Innovation (Grant No. PGC2018-096444-B-I00 and PID2021-122839NB-I00). J.F.E.C. gratefully acknowledges support from the Dodd-Walls Centre for Photonic and Quantum Technologies.

- [2] Krems, R. V. Cold controlled chemistry. *Phys. Chem. Chem. Phys.* 10, 4079–4092 (2008).
- [3] Stuhl, B. K., Hummon, M. T. & Ye, J. Cold stateselected molecular collisions and reactions. *Annu. Rev. Phys. Chem.* 65, 501–518 (2014).
- [4] Balakrishnan, N. Perspective: Ultracold molecules and the dawn of cold controlled chemistry. J. Chem. Phys. 145, 150901 (2016).
- [5] Bohn, J. L., Rey, A. M. & Ye, J. Cold molecules: Progress in quantum engineering of chemistry and quantum matter. *Science* 357, 1002–1010 (2017).
- [6] Anderegg, L. et al. An optical tweezer array of ultracold molecules. Science 365, 1156–1158 (2019).
- [7] Toscano, J., Lewandowski, H. J. & Heazlewood, B. R. Cold and controlled chemical reaction dynamics. *Phys. Chem. Chem. Phys.* 22, 9180–9194 (2020).
- [8] Liu, Y. & Ni, K.-K. Bimolecular chemistry in the ultracold regime. Annu. Rev. Phys. Chem. 73, 73–96 (2022).
- [9] Heazlewood, B. R. & Softley, T. P. Towards chemistry at absolute zero. Nat. Rev. Chem. 5, 125–140 (2021).
- [10] Kendrick, B. K. et al. Non-adiabatic quantum interference in the ultracold Li +LiNa → Li₂ + Na reaction. Phys. Chem. Chem. Phys. 23, 5096-5112 (2021).
- [11] Hu, M.-G. et al. Nuclear spin conservation enables stateto-state control of ultracold molecular reactions. Nature Chemistry 13, 435–440 (2021).
- [12] Liu, Y. et al. Precision test of statistical dynamics with state-to-state ultracold chemistry. Nature 593, 379–384 (2021).
- [13] Anderegg, L. et al. Laser cooling of optically trapped molecules. Nature Physics 14, 890–893 (2018).
- [14] Blackmore, J. A. et al. Ultracold molecules for quantum simulation: rotational coherences in CaF and RbCs. Quantum Sci. Technol. 4, 014010 (2018).
- [15] Cheuk, L. W. et al. Observation of collisions between two ultracold ground-state caf molecules. Phys. Rev. Lett. 125, 043401 (2020).
- [16] Aggarwal, P. et al. Deceleration and trapping of srf molecules. Phys. Rev. Lett. 127, 173201 (2021).
- [17] Jurgilas, S. et al. Collisions between ultracold molecules and atoms in a magnetic trap. Phys. Rev. Lett. 126, 153401 (2021).
- [18] Yang, D., Huang, J., Hu, X., Xie, D. & Guo, H. Statistical quantum mechanical approach to diatom-diatom capture dynamics and application to ultracold KRb + KRb reaction. J. Chem. Phys. 152, 241103 (2020).
- [19] Croft, J. F. E., Bohn, J. L. & Quéméner, G. Unified model of ultracold molecular collisions. *Phys. Rev. A* 102, 033306 (2020).
- [20] Perreault, W. E., Mukherjee, N. & Zare, R. N. Quantum control of molecular collisions at 1 kelvin. *Science* 358, 356–359 (2017).
- [21] Perreault, W. E., Mukherjee, N. & Zare, R. N. Cold quantum-controlled rotationally inelastic scattering of HD with H₂ and D₂ reveals collisional partner reorientation. *Nat. Chem.* 10, 561–567 (2018).
- [22] Perreault, W. E., Mukherjee, N. & Zare, R. N. $\mathrm{HD}(v=1,\ j=2,\ m)$ orientation controls HD-He rotationally inelastic scattering near 1 K. J. Chem. Phys. **150**, 174301 (2019).
- [23] Zhou, H., Perreault, W. E., Mukherjee, N. & Zare, R. N. Shape resonance determined from angular distribution in D_2 (v=2, j=2) + He \rightarrow D_2 (v=2, j=0) + He cold scattering. *J. Chem. Phys* **154**, 104309 (2021).

- [24] Zhou, H., Perreault, W. E., Mukherjee, N. & Zare, R. N. Quantum mechanical double slit for molecular scattering. *Science* 374, 960–964 (2021).
- [25] Perreault, W. E., Zhou, H., Mukherjee, N. & Zare, R. N. Coherent preparation of highly vibrating and rotating D₂ molecules. J. Phys. Chem. Lett 13, 4682–4687 (2022).
- [26] Zhou, H., Perreault, W. E., Mukherjee, N. & Zare, R. N. Anisotropic dynamics of resonant scattering between a pair of cold aligned diatoms. *Nat. Chem.* 14, 658–663 (2022).
- [27] Jambrina, P. G. et al. Stereodynamical control of cold collisions between two aligned D_2 molecules (2022). ArXiv:2207.10064v1.
- [28] Zuo, J., Croft, J. F. E., Yao, Q., Balakrishnan, N. & Guo, H. Full-dimensional potential energy surface for ro-vibrationally inelastic scattering between H₂ molecules. J. Chem. Theory Comput. 17, 6747-6756 (2021).
- [29] Green, S. Rotational excitation in H₂-H₂ collisions: Close-coupling calculations. J. Chem. Phys. 62, 2271–2277 (1975).
- [30] Zarur, G. & Rabitz, H. Effective potential formulation of molecule-molecule collisions with application to H₂-H₂. J. Chem. Phys. 60, 2057-2078 (1974).
- [31] Flower, D. R. The rotational excitation of H₂ by H₂. Mon. Not. Royal Astron. Soc. 297, 334–336 (1998).
- [32] Flower, D. R. & Roueff, E. Rovibrational relaxation in collisions between H₂ molecules: I. transitions induced by ground state para-H₂. J. Phys. B: At. Mol. Opt. Phys 31, 2935–2947 (1998).
- [33] Flower, D. R. & Roueff, E. Rovibrational relaxation in collisions between H₂ molecules: II. influence of the rotational state of the perturber. J. Phys. B: At. Mol. Opt. Phys 32, 3399–3407 (1999).
- [34] Schwenke, D. W. Calculations of rate constants for the three-body recombination of H₂ in the presence of H₂. J. Chem. Phys. 89, 2076–2091 (1988).
- [35] Lee, T.-G. et al. Rotational quenching rate coefficients for H₂ in collisions with H₂ from 2 to 10,000 K. The Astrophysical Journal 689, 1105–1111 (2008).
- [36] Diep, P. & Johnson, J. K. An accurate H₂–H₂ interaction potential from first principles. J. Chem. Phys. 112, 4465– 4473 (2000).
- [37] Diep, P. & Johnson, J. K. Erratum: "an accurate H₂-H₂ interaction potential from first principles" [j. chem. phys. 112, 4465 (2000)]. J. Chem. Phys. 113, 3480-3481 (2000).
- [38] Pogrebnya, S. K. & Clary, D. C. A full-dimensional quantum dynamical study of vibrational relaxation in H₂+H₂. Chem. Phys. Lett. **363**, 523 528 (2002).
- [39] Boothroyd, A. I., Dove, J. E., Keogh, W. J., Martin, P. G. & Peterson, M. R. Accurate ab initio potential energy computations for the H₄ system: Tests of some analytic potential energy surfaces. J. Chem. Phys. 95, 4331–4342 (1991).
- [40] Lin, S. Y. & Guo, H. Full-dimensional quantum wave packet study of rotationally inelastic transitions in H₂+H₂ collision. J. Chem. Phys. 117, 5183-5191 (2002).
- [41] Lin, S. Y. & Guo, H. Full-dimensional quantum wave packet study of collision-induced vibrational relaxation between para-H₂. Chem. Phys. 289, 191–199 (2003).
- [42] Lin, S. Y. & Guo, H. Full-dimensional wave packet studies of collisional vibrational relaxation of both p- and o-H₂. J. Phys. Chem. A 107, 7197–7203 (2003).
- [43] Gatti, F., Otto, F., Sukiasyan, S. & Meyer, H.-D. Rotational excitation cross sections of para-H₂+para-H₂ colli-

- sions. a full-dimensional wave-packet propagation study using an exact form of the kinetic energy. *J. Chem. Phys.* **123**, 174311 (2005).
- [44] Panda, A. N., Otto, F., Gatti, F. & Meyer, H.-D. Rovibrational energy transfer in ortho-H₂+para-H₂ collisions. J. Chem. Phys. 127, 114310 (2007).
- [45] Quéméner, G., Balakrishnan, N. & Krems, R. V. Vibrational energy transfer in ultracold molecule-molecule collisions. *Phys. Rev. A* 77, 030704 (2008).
- [46] Quéméner, G. & Balakrishnan, N. Quantum calculations of H₂-H₂ collisions: From ultracold to thermal energies. J. Chem. Phys. 130, 114303 (2009).
- [47] Hinde, R. J. A six-dimensional H₂-H₂ potential energy surface for bound state spectroscopy. J. Chem. Phys. 128, 154308 (2008).
- [48] Balakrishnan, N., Quéméner, G., Forrey, R. C., Hinde, R. J. & Stancil, P. C. Full-dimensional quantum dynamics calculations of H₂-H₂ collisions. *J. Chem. Phys.* 134, 014301 (2011).
- [49] dos Santos, S. F. et al. Quantum dynamics of rovibrational transitions in H₂-H₂ collisions: Internal energy and rotational angular momentum conservation effects. J. Chem. Phys. 134, 214303 (2011).
- [50] dos Santos, S. F., Balakrishnan, N., Forrey, R. C. & Stancil, P. C. Vibration-vibration and vibration-translation energy transfer in H₂-H₂ collisions: A critical test of experiment with full-dimensional quantum dynamics. *J. Chem. Phys.* 138, 104302 (2013).
- [51] Patkowski, K. et al. Potential energy surface for interactions between two hydrogen molecules. J. Chem. Phys. 129, 094304 (2008).
- [52] Wan, Y. et al. Collisional quenching of highly excited H₂ due to H₂ collisions. Astrophys. J 862, 132 (2018).
- [53] Hernández, M. I., Tejeda, G., Fernández, J. M. & Montero, S. Rate coefficients for H₂:H₂ inelastic collisions in the ground vibrational state from 10 to 1000 K. A&A 647, A155 (2021).
- [54] Johnson, D. L., Grace, R. S. & Skofronick, J. G. The total scattering cross sections for H₂+H₂, D₂+D₂, and HD+HD for relative collision energies below 10 meV. J. Chem. Phys. 71, 4554–4569 (1979).
- [55] Schaefer, J. & Meyer, W. Theoretical studies of H₂-H₂ collisions. i. elastic scattering of ground state para- and ortho-H₂ in the rigid rotor approximation. *J. Chem. Phys.* 70, 344–360 (1979).
- [56] Montero, S. & Pérez-Ríos, J. Rotational relaxation in molecular hydrogen and deuterium: Theory versus acoustic experiments. J. Chem. Phys. 141, 114301 (2014).
- [57] Krems, R. TwoBC quantum scattering program, University of British Columbia, Vancouver, Canada, 2006.
- [58] Arthurs, A. M. & Dalgarno, A. the theory of scattering by a rigid rotator. *Proc. Roy. Soc. London, Ser. A* 256, 540–551 (1960).
- [59] Takayanagi, K. The production of rotational and vibrational transitions in encounters between molecules. vol. 1 of Adv. At. Mol. Phys., 149 – 194 (Academic Press, 1965).
- [60] Green, S. Rotational excitation in H₂-H₂ collisions: Close-coupling calculations. J. Chem. Phys. 62, 2271–2277 (1975).
- [61] Alexander, M. H. & DePristo, A. E. Symmetry considerations in the quantum treatment of collisions between two diatomic molecules. J. Chem. Phys. 66, 2166–2172

- (1977).
- [62] Balakrishnan, N., Croft, J. F. E., Yang, B. H., Forrey, R. C. & Stancil, P. C. Rotational quenching of HD in collisions with H₂: Resolving discrepancies for low-lying rotational transitions. *Astrophys. J* 866, 95 (2018).
- [63] Croft, J. F. E., Balakrishnan, N., Huang, M. & Guo, H. Unraveling the stereodynamics of cold controlled HD-H₂ collisions. *Phys. Rev. Lett.* 121, 113401 (2018).
- [64] Croft, J. F. E. & Balakrishnan, N. Controlling rotational quenching rates in cold molecular collisions. *J. Chem. Phys.* 150, 164302 (2019).
- [65] Jambrina, P. G. et al. Stereodynamical control of a quantum scattering resonance in cold molecular collisions. Phys. Rev. Lett. 123, 043401 (2019).
- [66] Monchick, L. & Schaefer, J. Theoretical studies of H₂-H₂ collisions. II. scattering and transport cross sections of hydrogen at low energies: Tests of a new ab initio vibrotor potential. J. Chem. Phys. 73, 6153-6161 (1980).
- [67] Huo, W. M. & Green, S. Quantum calculations for rotational energy transfer in nitrogen molecule collisions. J. Chem. Phys. 104, 7572–7589 (1996).
- [68] Avdeenkov, A. V. & Bohn, J. L. Ultracold collisions of oxygen molecules. Phys. Rev. A 6405, 052703 (2001).
- [69] Takayanagi, K. Vibrational and rotational transitions in molecular collisions. Supp. Prog. Theo. Phys. 25, 1–98 (1963).
- [70] Rabitz, H. & Lam, S. Rotational energy relaxation in molecular hydrogen. J. Chem. Phys. 63, 3532–3542 (1975).
- [71] Danby, G., Flower, D. R. & Monteiro, T. S. Rotationally inelastic collisions between H₂ molecules in interstellar magnetohydrodynamical shocks. *Mon. Not. Royal Astron. Soc.* 226, 739–745 (1987).
- [72] Tscherbul, T. V., Suleimanov, Y. V., Aquilanti, V. & Krems, R. V. Magnetic field modification of ultracold molecule-molecule collisions. New J. Phys. 11, 055021 (2009).
- [73] Stoof, H. T. C., Koelman, J. M. V. A. & Verhaar, B. J. Spin-exchange and dipole relaxation rates in atomic hydrogen: rigorous and simplified calculations. *Phys. Rev. B* 38, 4688–4697 (1988).
- [74] Burke Jr, J. P. Theoretical investigation of cold alkali atom collisions (University of Colorado at Boulder, 1999).
- [75] Manolopoulos, D. E. An improved log-derivative method for inelastic scattering. J. Chem. Phys. 85, 6425–6429 (1986).
- [76] Bethe, H. A. Theory of disintegration of nuclei by neutrons. Phys. Rev. 47, 747–759 (1935).
- [77] Wigner, E. P. on the behavior of cross sections near thresholds. Phys. Rev. 73, 1002–1009 (1948).
- [78] Simbotin, I. & Côté, R. Jost function description of near threshold resonances for coupled-channel scattering. *Chem. Phys.* 462, 79–93 (2015). Inelastic Processes in Atomic, Molecular and Chemical Physics.
- [79] Mukherjee, N. & Zare, R. N. Stark-induced adiabatic raman passage for preparing polarized molecules. J. Chem. Phys. 135, 024201 (2011).
- [80] Jambrina, P. G., González-Sánchez, L., Lara, M., Menéndez, M. & Aoiz, F. J. Unveiling shape resonances in H + HF collisions at cold energies. *Phys. Chem. Chem. Phys.* 22, 24943–24950 (2020).